

# Helium-4 gravitational form factors: exchange currents

Fangcheng He<sup>1,\*</sup> and Ismail Zahed<sup>1,†</sup>

<sup>1</sup>*Center for Nuclear Theory, Department of Physics and Astronomy,  
Stony Brook University, Stony Brook, New York 11794, 3800, USA*

(Dated: June 12, 2024)

We evaluate the leading exchange corrections to the Helium-4 gravitational form factors (GFFs) upto momenta of the order of the nucleon mass. We use both the K-harmonic method with simple pair nucleon potential, and a Jastrow trial function using the Argonne  $v_{14}$  potential, to evaluate the Helium-4 GFFs. The exchange current contributions include the pair interaction, plus the seagull and the pion exchange interactions, modulo the recoil corrections. To estimate the off-shellness of the pion nucleon coupling in this momenta range, we discuss the results using either the pseudo-scalar (PS) or pseudo-vector (PV) pion-nucleon couplings. When the PV coupling is used, the pair diagram contribution is higher order in the non-relativistic expansion. The results for the Helium-4 A-GFF are comparable to those given by the impulse approximation, especially for the PS coupling using both the K-Harmonic method and variational method. The exchange current contributions with the PS coupling for the charge form factor of Helium-4, yield better agreement with the existing data over a broad range of momenta, especially when the Argonne  $v_{14}$  potential including the D-wave admixture is used.

## I. INTRODUCTION

The gravitational form factors (GFFs) of hadrons carry important information on their mass and spin structure. Recent lattice QCD simulations of the pion and nucleon GFFs have started to show how the quarks and gluons compose these form factors [1–3]. This has led to a better understanding of the internal properties of these hadrons [4, 5], beyond their standard electromagnetic properties [6].

Recent measurements of threshold photoproduction of charmonium off nucleons by two collaborations at JLab [7, 8], have given a first empirical estimate of nucleon gluonic GFFs, with the help of model analyses [9, 10]. These measurements complement the quark GFFs extracted from deeply virtual Compton scattering also at Jlab [11]. The combined empirical and numerical estimates of the nucleon GFFs, allow for a better understanding of the mass and stress distribution inside the nucleon [12–17]. In particular, the mass radius of the nucleon was found to be smaller than the electromagnetic radius, as suggested initially in dual gravity [12, 18]. Similar understanding is being also reached for the pion [19–29].

Nuclei are composed of nucleons bound by strong

interactions. Most of our understanding of nuclei follows from decades of electromagnetic scattering [30], showing that the electric and magnetic form factors receive sizable contributions from mesonic exchange currents in a wide range of momenta [31]. Furthermore, electron and muon scattering on nuclei have also shown that the quark sub-constituents of the nucleon in nuclei get modified through shadowing (large Bjorken- $x$ ) and anti-shadowing (small Bjorken- $x$ ). However, it is less clear how the gluon sub-constituents are being affected in nuclei. Coherent photoproduction of phi-mesons off the deuteron by the CLAS collaboration [32] and LEPS collaborations [33], have not added more insights beyond those expected from two loosely bound nucleons.

Helium-4 is the lightest nucleus with strongly bound nucleons. It is a spin-isospin singlet with a well measured electromagnetic form factor, mass and charge radius. Recently we have shown that the Helium-4 GFFs in the impulse approximation, deviate from those of independent nucleons in a range of momenta within the nucleon mass [34]. Similar observations were made using the Skyrme model [35]. However, it is known that meson exchange-current contributions to the electromagnetic form factors are important [36–39]. The purpose of this work is to address these exchanges for the Helium-4 GFFs. For completeness, we note the light cone analysis of the deuteron GFFs in [40].

This paper is a follow up on our recent analy-

\* fangcheng.he@stonybrook.edu

† ismail.zahed@stonybrook.edu

sis of the EMT of light nuclei in the impulse approximation [34, 41]. In section II we briefly detail the ground state wavefunctions for the description of Helium-4 using the K-harmonic method with no D-wave admixture, and the variational method using the Argonne *v*14 potential with D-wave admixture. In section III we describe the exchange current contributions to the GFFs of Helium-4, and their generic matrix elements with both wavefunctions. In section IV we explicitly evaluate all exchange matrix elements for Helium-4 using the wavefunction from the K-harmonic method. Those from the variational method are multi-dimensional and are evaluated numerically using Monte Carlo method. The numerical results are discussed in section V. Our conclusions are in section VI. In the Appendices we list the numerical results for the variational wavefunction for future use, and apply the same analysis for the Helium-4 charge form factor for comparison.

## II. GROUND STATE OF HELIUM-4

In this section we briefly outline the construction of the ground state wavefunction of Helium-4, using two methods. The first method makes use of the Reid nucleon pair potential and K-harmonics in the hyper-radius approximation, without D-wave contribution. We recently used for the analysis of the GFFs of Helium-4 in the impulse approximation [34]. The second method, makes use of the Argonne *v*14 nucleon pair potentials, retaining the D-wave contribution [42].

### A. K-Harmonic Method

The essential aspects of the radial part of the ground state of Helium-4 using the K-harmonic method in the hyper-radius approximation was discussed recently in [34] (and references therein). More specifically, the 4 nucleons in the  $0^{++}$  spin-isospin configurations are described by

$$\Phi_H[1, \dots, 4] = \varphi[r_1, r_2, r_3, r_4] \Phi[\sigma, \tau], \quad (1)$$

with  $\Phi$  refers to the properly symmetrized spin-isospin wavefunction. To remove the spurious center of mass motion in Eq. (1), the nucleon coordinates in (1) are split into three Jacobi coordinates  $\vec{\xi}_{1,2,3}$  plus the center of mass  $\vec{R}_C$

$$\begin{aligned} \vec{\xi}_1 &= \frac{1}{\sqrt{2}}(\vec{r}_2 - \vec{r}_1), \\ \vec{\xi}_2 &= \frac{1}{\sqrt{6}}(\vec{r}_1 + \vec{r}_2 - 2\vec{r}_3), \\ \vec{\xi}_3 &= \frac{1}{2\sqrt{3}}(\vec{r}_1 + \vec{r}_2 + \vec{r}_3 - 3\vec{r}_4), \\ \vec{R}_C &= \frac{1}{4}(\vec{r}_1 + \vec{r}_2 + \vec{r}_3 + \vec{r}_4), \end{aligned} \quad (2)$$

with the radial hyperdistance

$$R^2 = \frac{1}{4} \sum_{i \neq j} (\vec{r}_i - \vec{r}_j)^2 = \vec{\xi}_1^2 + \vec{\xi}_2^2 + \vec{\xi}_3^2. \quad (3)$$

To keep this analysis simple as in [34], we will ignore the D-wave contribution. Its role will be detailed in the second analysis to follow, using the Argonne potential below. With this in mind, the radial eigenstates carry constant hyper-spherical harmonic, with the spin-isospin content [43]

$$\begin{aligned} \Phi[\sigma, \tau] &= \frac{\sqrt{105}}{8\pi^2} \left( ([\sigma(1), \sigma(2)]_1 [\sigma(3), \sigma(4)]_1)_{00} ([\tau(1), \tau(2)]_0 [\tau(3), \tau(4)]_0)_{00} \right. \\ &\quad \left. - ([\sigma(1), \sigma(2)]_0 [\sigma(3), \sigma(4)]_0)_{00} ([\tau(1), \tau(2)]_1 [\tau(3), \tau(4)]_1)_{00} \right). \end{aligned} \quad (4)$$

The form of Eq. (1) in hyper-spherical coordinates can be expressed as

$$\Phi_H[1, \dots, 4] = \varphi[R] \Phi[\sigma, \tau]. \quad (5)$$

The radial part  $\varphi[R] = u(R)/R^4$  where  $u(R)$  is the reduced wavefunction, solves

$$u'' - \frac{12}{R^2}u - \frac{2m_N}{\hbar^2}(W(R) + V_C(R) - E)u = 0, \quad (6)$$

Here  $W(R)$  and  $V_C$  represent the pair nucleon and Coulomb potentials, which can be written as [34, 43]

$$\begin{aligned} W(R) &= \frac{315}{4} \int_0^1 dx (1-x^2)^2 x^2 V(\sqrt{2}Rx), \\ V_C(R) &= \frac{2.23\text{MeVfm}}{R}, \end{aligned} \quad (7)$$

with

$$V(r) = +1310.21 e^{-(r/0.7)^2} - 467.97 e^{-(r/1.16)^2}. \quad (8)$$

The radial solution to Eq. (6) is shown in the top panel in Fig. 1. The ensuing wavefunction reproduces the correct binding energy and charge radius of Helium-4. It also describes fairly well the empirical charge form factor of Helium-4 up-to momentum of the order of half the nucleon mass [34].

### B. Argonne *v14* variational method

To include the D-wave contribution and more realistic nucleon pair interactions in Helium-4, we will make use of the Argonne *v14* symmetrized ( $\mathcal{S}$ ) variational wavefunction [44–46]

$$|\Psi_v\rangle = \mathcal{S} \prod_{i<j} (1 + U_{ij}) |\Psi_J\rangle, \quad (9)$$

with the Jastrow trial state

$$|\Psi_J\rangle = \prod_{i<j} f_c(r_{ij}) |\Phi\rangle,$$

where  $f_c(r)$  is a central pair correlation function, and  $\Phi$  the antisymmetric spin-isospin wavefunction in Eq. (4). The pair correlation functions  $U_{ij}$  built in the variational state, is valued in the set of operators making up the Argonne *v14* potential

$$U_{ij} = \sum_{p=2}^m u_p(r_{ij}) O_{ij}^p, \quad (10)$$

with  $O_{ij}^p$  making up the 14 spin-isospin pair operators in the *v14* potential [44–46]

$$\begin{aligned} O_{ij}^{p=1,14} &= 1, \tau_i \cdot \tau_j, \sigma_i \cdot \sigma_j, (\tau_i \cdot \tau_j)(\sigma_i \cdot \sigma_j), S_{ij}, \\ &S_{ij}(\tau_i \tau_j), \vec{L} \cdot \vec{S}, \vec{L} \cdot \vec{S}(\tau_i \tau_j), \vec{L}^2, \vec{L}^2(\tau_i \cdot \tau_j), \\ &\vec{L}^2(\sigma_i \cdot \sigma_j), \vec{L}^2(\sigma_i \cdot \sigma_j)(\tau_i \cdot \tau_j), \\ &(\vec{L} \cdot \vec{S})^2, (\vec{L} \cdot \vec{S})^2(\tau_i \tau_j). \end{aligned} \quad (11)$$

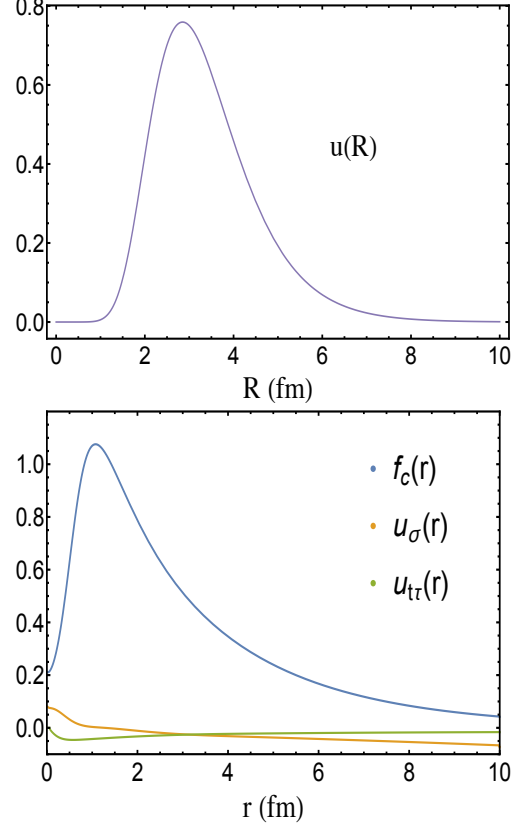


FIG. 1: Top: The reduced wave function used in K-Harmonic Method; Bottom: Helium-4 partial wave-functions following from the use of the Argonne *v14* potential [44]: central  $f_c(r)$  (solid-blue), spin  $u_\sigma(r)$  (solid-orange) and isospin-tensor  $u_{t\tau}$  (solid-green).

Numerically the trial functions  $u_p(r_{ij})$  will turn out to be small, which allows us to simplify Eq. (9)

$$|\Psi_v\rangle = (1 + \sum_{i<j} U_{ij}) |\Psi_J\rangle. \quad (12)$$

Using the spin-isospin identities [45]

$$\begin{aligned} \tau_i \cdot \tau_j |\Phi\rangle &= -(2 + \sigma_i \cdot \sigma_j) |\Phi\rangle, \\ (\tau_i \cdot \tau_j)(\sigma_i \cdot \sigma_j) |\Phi\rangle &= -3 |\Phi\rangle, \\ S_{ij}(\tau_i \cdot \tau_j) |\Phi\rangle &= -3 S_{ij} |\Phi\rangle, \\ (\vec{L} \cdot \vec{S}) |\Phi\rangle &= \vec{L}^2 |\Phi\rangle = 0. \end{aligned} \quad (13)$$

To include the central three body correlation, the pair correlation function can be modified as follows [44–46].

$$u_p(r_{ij}) \rightarrow \mathcal{F}_{ij} u_p(r_{ij}) = [\prod_{k \neq i,j} f_{ijk}] u_p(r_{ij}), \quad (14)$$

where  $f_{ijk}$  is chosen to be [44]

$$f_{ijk} = 1 - 9 \left( \frac{r_{ij}}{r_{ij} + r_{ik} + r_{jk}} \right)^4 \times \exp[-0.1(r_{ij} + r_{ik} + r_{jk})], \quad (15)$$

we can rewrite Eq. (12) in the form

$$|\Psi_v\rangle = \left\{ 1 + \sum_{i < j} \mathcal{F}_{ij} [u_\sigma(r_{ij})\sigma_i \cdot \sigma_j + u_{t\tau}(r_{ij})S_{ij}\tau_i \cdot \tau_j] \right\} |\Psi_J\rangle. \quad (16)$$

The Jastrow pair correlation function  $f(r)$  and the operator correlation functions  $u_{\sigma,t\tau}$ , can be repacked in Eq. (16), in terms of their contributions to the singlet and triplet spin and isospin channels, using the identity [44, 46]

$$f_c(r_{ij}) [1 + u_\sigma(r_{ij})\sigma_i \cdot \sigma_j + u_{t\tau}(r_{ij})\sigma_i \cdot \sigma_j] |\Phi\rangle = \left( \sum_{S,T} f_{S,T}(r_{ij}) P_S P_T + f_{t,0}(r_{ij}) S_{ij} P_{T=0} \right) |\Phi\rangle \quad (17)$$

$$\begin{aligned} -\frac{\hbar^2}{m} [r f_{0,1}(r)]'' + (\bar{v}_{0,0} + \lambda_{0,T}) f_{0,1}(r) r &= 0, \\ -\frac{\hbar^2}{m} [r f_{1,0}(r)]'' + (\bar{v}_{1,0} + \lambda_{1,0}) f_{1,0}(r) r + 8(\bar{v}_{t,0} + \lambda_{t,0}) f_{t,0}(r) r &= 0, \\ -\frac{\hbar^2}{m} [(r f_{t,0}(r))'' - \frac{6}{r^2} (r f_{t,0}(r))] + (\bar{v}_{t,0} + \lambda_{t,0}) f_{1,0}(r) r \\ + (\bar{v}_{t,0} + \lambda_{t,0} - 2(\bar{v}_{t,0} + \lambda_{t,0}) - 3(\bar{v}_{b,0} + \lambda_{b,0}) + 6\bar{v}_{q1,0} + q\bar{v}_{bb,0}) f_{t,0}(r) r &= 0, \end{aligned} \quad (20)$$

here  $\bar{v}_{S,T}$  refer to the explicit  $v14$  pair nucleon potentials. The eigenvalues  $\lambda_{S,T}$  include the screening effects at short distances, and their behavior at large distances is fixed by the asymptotic of the correlation functions. We refer to [42, 44] for their explicit form. In Fig 1 we show our numerical results for  $f_c$ ,  $u_\sigma$  and  $u_{t\tau}$ , which are in overall agreement with those reported in [44]. In appendix. A, we have tabulated our results for future comparison.

### III. EXCHANGE CURRENTS IN HELIUM-4

Helium-4 gravitational form factors in the impulse approximation were discussed in [34]. In this section we extend the analysis to the exchange currents, following our recent discussion in the deuteron

Here  $P_S$  and  $P_T$  are the spin and isospin projection operators, i.e.

$$\begin{aligned} P_{S=1} &= (3 + \sigma_i \cdot \sigma_j)/4, \\ P_{S=0} &= (1 - \sigma_i \cdot \sigma_j)/4, \\ P_{T=1} &= (3 + \tau_i \cdot \tau_j)/4, \\ P_{T=0} &= (1 - \tau_i \cdot \tau_j)/4. \end{aligned} \quad (18)$$

The pair correlation functions  $f_c$ ,  $u_\sigma$  and  $u_{t\tau}$  can be related to the projected functions through

$$\begin{aligned} f_c &= \frac{1}{4}(3f_{1,0} + f_{0,1}), \\ u_\sigma &= \frac{1}{4}(f_{1,0} - f_{0,1})/f_c, \\ u_{t\tau} &= -\frac{1}{3}f_{t,0}/f_c, \end{aligned} \quad (19)$$

where we made use of Eq. (13). In the ground state of Helium-4 with  $L = 0$ , the spin-isospin projected functions  $f_{S,T}$  and spin-singlet-tensor function  $f_{t,0}$  can be obtained by solving the coupled Schrodinger equations [44]

case [41]. More specifically, the gravitational exchange contributions to Helium-4 in the single pion exchange approximation are illustrated in Fig. 2. We will refer to them generically by  $T_X^{\mu\nu}$  with the pair contribution (a), the seagull contribution (b), the pion exchange contribution (c) and the recoil corrections plus wavefunction renormalization (d). For a further assessment of the off-shellness effects between the pion-nucleon pseudoscalar and pseudovector couplings, we will discuss both, where we note that the seagull contribution (c) is absent for the former coupling. The explicit operator forms for each of these contributions are quoted in section IV below.

### A. Matrix element: K-harmonic method

The generic structure of the matrix element in the K-harmonic method, can be recast into a multi-

$$\begin{aligned}
& \left\langle +\frac{k}{2}m' \left| T_X^{\mu\nu} \right| -\frac{k}{2}m \right\rangle \\
&= \int d^3\xi_1 \int d^3\xi_2 \int d^3\xi_3 \frac{d^3q_2}{(2\pi)^3} \\
&\times \mathbf{exp} \left[ -i\sqrt{2}\vec{q}_2\vec{\xi}_1 + i\vec{k} \left( \frac{\vec{\xi}_1}{\sqrt{2}} - \frac{\vec{\xi}_2}{\sqrt{6}} - \frac{\vec{\xi}_3}{2\sqrt{3}} \right) \right] \langle \Phi_H[\xi] | T_X^{\mu\nu}(\sigma_1, \sigma_2) | \Phi_H[\xi] \rangle + \text{permutation}
\end{aligned} \tag{21}$$

with  $\vec{q}_2$  the momentum of exchanged pion in Fig. 2. The argument of the Fourier transform refers to the struck nucleon relative to the center of mass coordinate, i.e.

$$\frac{\vec{\xi}_1}{\sqrt{2}} - \frac{\vec{\xi}_2}{\sqrt{6}} - \frac{\vec{\xi}_3}{2\sqrt{3}} = \vec{R}_C - \vec{r}_1 \tag{22}$$

$T_X^{\mu\nu}$  is short for the inserted EMT operators in Fig. 2. Their explicit non-relativistic forms are listed in Eqs. (27), (33), (36) and (39) for the pair contri-

dimensional integral over the Jacobi coordinates

bution, the seagull contribution, the pion exchange contribution and recoil contribution, respectively. To keep the hyperspherical symmetric, the Jacobi coordinates are set to be

$$\begin{aligned}
\xi_1 &= R \cos\theta (\sin\theta_1 \cos\phi_1, \sin\theta_1 \sin\phi_1, \cos\theta_1), \\
\xi_2 &= R \sin\theta \cos\phi (\sin\theta_2 \cos\phi_2, \sin\theta_2 \sin\phi_2, \cos\theta_2), \\
\xi_3 &= R \sin\theta \sin\phi (\sin\theta_3 \cos\phi_3, \sin\theta_3 \sin\phi_3, \cos\theta_3),
\end{aligned} \tag{23}$$

The above integral can be reduced after integrating over the angular

$$\begin{aligned}
& \left\langle +\frac{k}{2}m' \left| T_X^{\mu\nu} \right| -\frac{k}{2}m \right\rangle \\
&= \int_0^\infty dR \int_0^{\frac{\pi}{2}} d\theta \sin\theta^5 \cos\theta^2 \int_0^{\frac{\pi}{2}} d\phi \sin\phi^2 \cos\phi^2 \int d\Omega_2 \mathbf{exp} \left[ -i\vec{k} \frac{\vec{\xi}_2}{\sqrt{6}} \right] \int d\Omega_3 \mathbf{exp} \left[ -i\vec{k} \frac{\vec{\xi}_3}{2\sqrt{3}} \right] \\
&\times \int \frac{d^3q_2}{(2\pi)^3} \int d\Omega_1 \mathbf{exp} \left[ -i\sqrt{2}\vec{q}_2\vec{\xi}_1 + i\vec{k} \frac{\vec{\xi}_1}{\sqrt{2}} \right] u(R)^2 \langle \Phi | T_X^{\mu\nu}(\sigma_1, \sigma_2) | \Phi \rangle + \text{permutation} \\
&= (4\pi)^2 \int_0^\infty dR \int_0^{\frac{\pi}{2}} d\theta \sin\theta^5 \cos\theta^2 \int_0^{\frac{\pi}{2}} d\phi \sin\phi^2 \cos\phi^2 j_0 \left( \frac{kR \sin\theta \cos\phi}{\sqrt{6}} \right) j_0 \left( \frac{kR \sin\theta \sin\phi}{2\sqrt{3}} \right) \\
&\times \int \frac{d^3q_2}{(2\pi)^3} \int d\Omega_1 \mathbf{exp} \left[ -i\sqrt{2}\vec{q}_2\vec{\xi}_1 + i\vec{k} \frac{\vec{\xi}_1}{\sqrt{2}} \right] u(R)^2 \langle \Phi | T_X^{\mu\nu}(\sigma_1, \sigma_2) | \Phi \rangle + \text{permutation},
\end{aligned} \tag{24}$$

### B. Matrix element: $v_{14}$ potential

The generic form of the exchange corrections, using the Argonne potential with the variational wave function (16) are of the form

$$\left\langle +\frac{k}{2}m' \left| T_{X\pi}^{\mu\nu} \right| -\frac{k}{2}m \right\rangle = \frac{1}{Z} \int d^3\vec{r}_{12} \int d^3\vec{r}_{13} \int d^3\vec{r}_{14} \frac{d^3q_2}{(2\pi)^3}$$

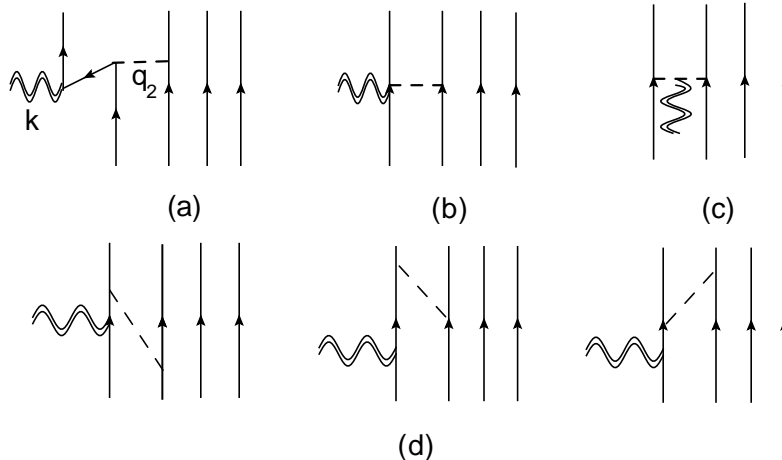


FIG. 2: Exchange contributions to the EMT: (a) The pair contribution, (b) seagull contribution, (c) pion exchange contribution, (d) recoil plus wave function renormalization. The solid, dashed and wavy lines represent the nucleon, pion and graviton, respectively. Note that there is no seagull contribution for a pseudoscalar pion-nucleon coupling.

$$\times \mathbf{exp} \left[ i\vec{q}_2 \cdot \vec{r}_{12} - i\vec{k} \cdot (\vec{r}_1 - \vec{R}_C) \right] \langle \Psi_v | T_X^{\mu\nu}(\sigma_1, \sigma_2) \Psi_v \rangle + \text{permutation}, \quad (25)$$

where  $\vec{r}_{ij} = \vec{r}_i - \vec{r}_j$ . Here  $Z$  enforces the wavefunction normalization

$$Z = \int d^3\vec{r}_{12} \int d^3\vec{r}_{13} \int d^3\vec{r}_{14} \langle \Psi_v | \Psi_v \rangle. \quad (26)$$

Note that we have switched back to initial coordinates  $\vec{r}_{12}$ ,  $\vec{r}_{13}$  and  $\vec{r}_{14}$  as integration variables, which tie to the Jacobi coordinates (2) by translational invariance, modulo a constant Jacobian. The latter can be eliminated in the ratio (25). To evaluate the multi-dimensional integral in Eq. (25), we will use the Monte Carlo method described in [44, 46].

#### IV. MATRIX ELEMENT OF EMT IN HELIUM-4

To extract the non-relativistic contributions to the exchange currents, we will make use of the diagrams in Fig. 2, with the positive nucleon contribution in (a) subtracted, and the recoil contribution and wavefunction renormalization in (d) retained. The wiggly line refers to the insertion of the EMT, and the dashed line to the pion exchange contribution using both pseudo-vector coupling and pseudo-scalar

coupling. Again, the explicit operator form for the EMT insertion  $T_X$  for nucleon pairs in the context of the impulse approximation, is given in [34] and to which we refer for completeness. Instead, we will give the explicit integral expressions for the form factors for each contribution, using the K-Harmonic Method only. Those from the Argonne  $v14$  will be evaluated numerically using Eq. (25) by Monte Carlo sampling, with only the final results given in section V.

##### A. Pair contribution

The EMT operator for the pair diagrams in Fig. 2a with pseudo-scalar coupling and pseudo-vector coupling, in the leading non-relativistic reduction read [41]

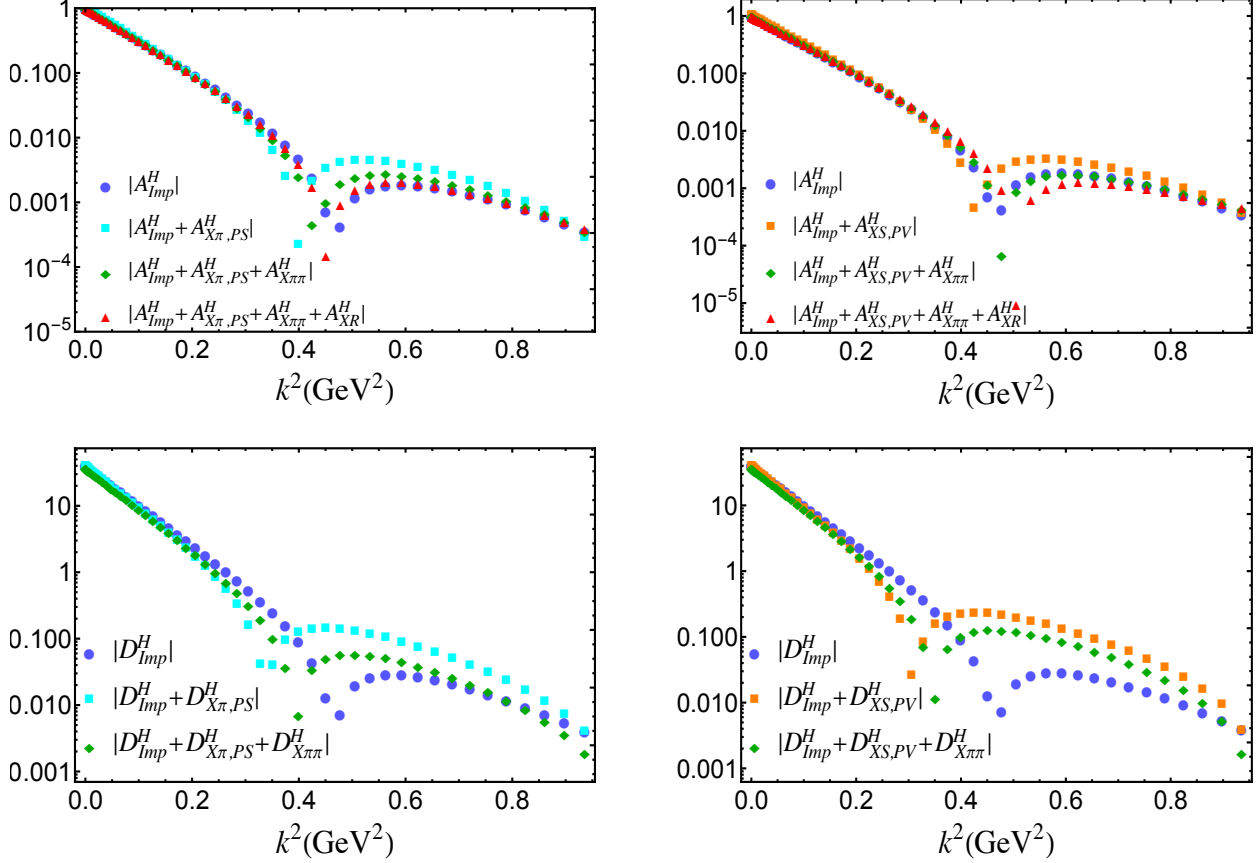


FIG. 3: Helium-4 GFFs with PS coupling (left) and PV coupling (right) using the K-Harmonics method: “imp” refers to the impulse approximation, “X $\pi$ ”, “XS”, “X $\pi\pi$ ” and “XR” refer to the exchange contributions in (Fig. 2a), seagull contribution in (Fig. 2b), pion exchange contribution in (Fig. 2c), and recoil contribution in (Fig. 2d), respectively.

$$T_{X\pi,PS}^{00}(k) = (A(k) + B(k)) \frac{g_{\pi N}^2}{(2m_N)^2} \tau_1 \cdot \tau_2 \frac{\vec{\sigma}_1 \cdot \vec{k} \vec{\sigma}_2 \cdot \vec{q}_2}{w_{q_2}^2} + (1 \leftrightarrow 2) + \mathcal{O}\left(\frac{g_{\pi N}^2}{m_N^4}\right) \quad (27a)$$

$$T_{X\pi,PS}^{ij}(k) = -A(k) \tau_1 \cdot \tau_2 \frac{g_{\pi N}^2}{(2m_N)^2} \frac{q_2^i \sigma_1^j + q_2^j \sigma_1^i}{2w_{q_2}^2} \vec{\sigma}_2 \cdot \vec{q}_2 + (1 \leftrightarrow 2) + \mathcal{O}\left(\frac{g_{\pi N}^2}{m_N^4}\right), \quad (27b)$$

$$T_{X\pi,PV}^{00,ij}(k) = \mathcal{O}\left(\frac{g_{\pi N}^2}{m_N^4}\right) \quad (27c)$$

$$(27d)$$

with the pion energy  $w_{q_2} = \sqrt{q_2^2 + m_\pi^2}$ . The GFFs  $A$  and  $D$  for Helium-4 are related to the matrix elements of  $T^{00}$  and  $T^{ij}$  through

$$\left\langle +\frac{k}{2} \left| T_{X\pi}^{00} \right| -\frac{k}{2} \right\rangle = (m_\alpha + \frac{k^2}{4m_\alpha}) A_{X\pi}^H + \frac{k^2}{4m_\alpha} D_{X\pi}^H,$$

$$\left\langle +\frac{k}{2} \left| T_{X\pi}^{ij} \right| -\frac{k}{2} \right\rangle = \frac{k_i k_j - \delta^{ij} k^2}{4m_\alpha} D_{X\pi}^H + \delta^{ij} D_{1,X\pi}^H.$$

Note that the term including  $D_{1,X\pi}^H$  breaks down the conservation law  $k^i T_{X\pi}^{ij} = 0$ . As noted in [41], all contributions in Fig. 2 need to be summed up, to uphold the conservation law. In particular, the contributions  $\delta^{ij}$  will be cancelled out. Therefore, we will not keep such a contribution in our following

(28)

calculation. With this in mind, the corresponding

GFFs for the pair diagrams with PS and PV coupling can be expressed as

$$A_{X\pi,PS}^H = -\frac{\vec{k}^2}{k^2 + 4m_\alpha^2} D_{X\pi,PS}^H + 6\frac{(4\pi)^2 g_{\pi N}^2}{(2m_N)^2} m_\pi^2 \int_0^\infty dR \int_0^{\frac{\pi}{2}} d\theta \int_0^{\frac{\pi}{2}} d\phi \mathbb{V} j_1\left(\frac{kR\cos\theta}{\sqrt{2}}\right) \frac{ku^2 Y_1^H}{6m_N} \times (A(k) + B(k)) \langle \Phi | \tau_1 \cdot \tau_2 \sigma_1 \cdot \sigma_2 | \Phi \rangle, \quad (29a)$$

$$D_{X\pi,PS}^H = 6\frac{(4\pi)^2 g_{\pi N}^2}{(2m_N)^2} m_\pi^2 \int_0^\infty dR \int_0^{\frac{\pi}{2}} d\theta \int_0^{\frac{\pi}{2}} d\phi \mathbb{V} j_2\left(\frac{kR\cos\theta}{\sqrt{2}}\right) \frac{-8m_\alpha m_\pi u^2 Y_2^H}{3k^2} A(k) \times \langle \Phi | \tau_1 \cdot \tau_2 \sigma_1 \cdot \sigma_2 | \Phi \rangle, \quad (29b)$$

$$A_{X\pi,PV}^H = D_{XS,PV}^H = \mathcal{O}\left(\frac{g_{\pi N}^2}{m_N^4}\right), \quad (29c)$$

where  $u(R)$  is the reduced hyper-radius wavefunction in Eq. (6), and factor  $\mathbb{V}$  is defined as

$$\mathbb{V} = \sin\theta^5 \cos\theta^2 \sin\phi^2 \cos\phi^2 j_0\left(\frac{kR \sin\theta \cos\phi}{\sqrt{6}}\right) j_0\left(\frac{kR \sin\theta \sin\phi}{2\sqrt{3}}\right), \quad (30)$$

with the shorthand Yukawa potentials,

$$\begin{aligned} Y_0^H &= e^{-m_\pi \sqrt{2}R \cos\theta} / (m_\pi \sqrt{2}R \cos\theta), \\ \bar{Y}_1^H &= (1 + 1/(m_\pi \sqrt{2}R \cos\theta)) Y_0^H, \\ Y_2^H &= (3/(m_\pi \sqrt{2}R \cos\theta)^2 + 3/(m_\pi \sqrt{2}R \cos\theta) + 1) Y_0^H. \end{aligned} \quad (31)$$

In the  $0^{++}$  Helium-4 ground state, we can use Eq. (4) to obtain

$$\langle \Phi | \tau_1 \cdot \tau_2 \sigma_1 \cdot \sigma_2 | \Phi \rangle = -\frac{315}{32\pi^4}. \quad (32)$$

### B. Seagull contribution

For the Seagull in Fig. 2(b), the EMT operator can be written as [41]

$$T_{XS,PV}^{00} = \mathcal{O}\left(\frac{g_{\pi N}^2}{m_N^4}\right), \quad (33a)$$

$$T_{XS,PV}^{ij} = -\tau_1 \cdot \tau_2 \frac{g_{\pi N}^2}{(2m_N)^2} \frac{q_2^i \sigma_1^j + q_2^j \sigma_1^i}{2w_{q_2}^2} \vec{\sigma}_2 \cdot \vec{q}_2 + (1 \leftrightarrow 2) + \mathcal{O}\left(\frac{g_{\pi N}^2}{m_N^4}\right). \quad (33b)$$

There is no contribution from the seagull diagram for the PS coupling case. Also the contribution to  $T_{XS}^{ij}$  from the PV coupling is equivalent to the contribution to  $T_{X\pi}^{ij}$  from the pair diagram for the PS coupling, with the exception of the extra nucleon GFF  $A(k)$  in Eq. (27b). The GFFs can be obtained using the following relations

$$\begin{aligned} \left\langle +\frac{k}{2} \left| T_{XS}^{00} \right| -\frac{k}{2} \right\rangle &= (m_\alpha + \frac{k^2}{4m_\alpha}) A_{XS}^H + \frac{k^2}{4m_\alpha} D_{XS}^H \\ &= \mathcal{O}\left(\frac{g_{\pi N}^2}{m_N^4}\right), \\ \left\langle +\frac{k}{2} \left| T_{XS}^{ij} \right| -\frac{k}{2} \right\rangle &= \frac{k_i k_j - \delta^{ij} k^2}{4m_\alpha} D_{XS}^H, \end{aligned} \quad (34)$$

where

$$A_{XS,PS}^H = D_{XS,PS}^H = 0, \quad (35a)$$

$$A_{XS,PV}^H = -\frac{\vec{k}^2}{k^2 + 4m_\alpha^2} D_{XS,PV}^H, \quad (35b)$$

$$D_{XS,PV}^H = 6\frac{(4\pi)^2 g_{\pi N}^2}{(2m_N)^2} m_\pi^2 \int_0^\infty dR \int_0^{\frac{\pi}{2}} d\theta \int_0^{\frac{\pi}{2}} d\phi \mathbb{V} j_2\left(\frac{kR\cos\theta}{\sqrt{2}}\right) \frac{-8m_\alpha m_\pi u^2 Y_2^H}{3k^2} \times \langle \Phi | \tau_1 \cdot \tau_2 \sigma_1 \cdot \sigma_2 | \Phi \rangle. \quad (35c)$$



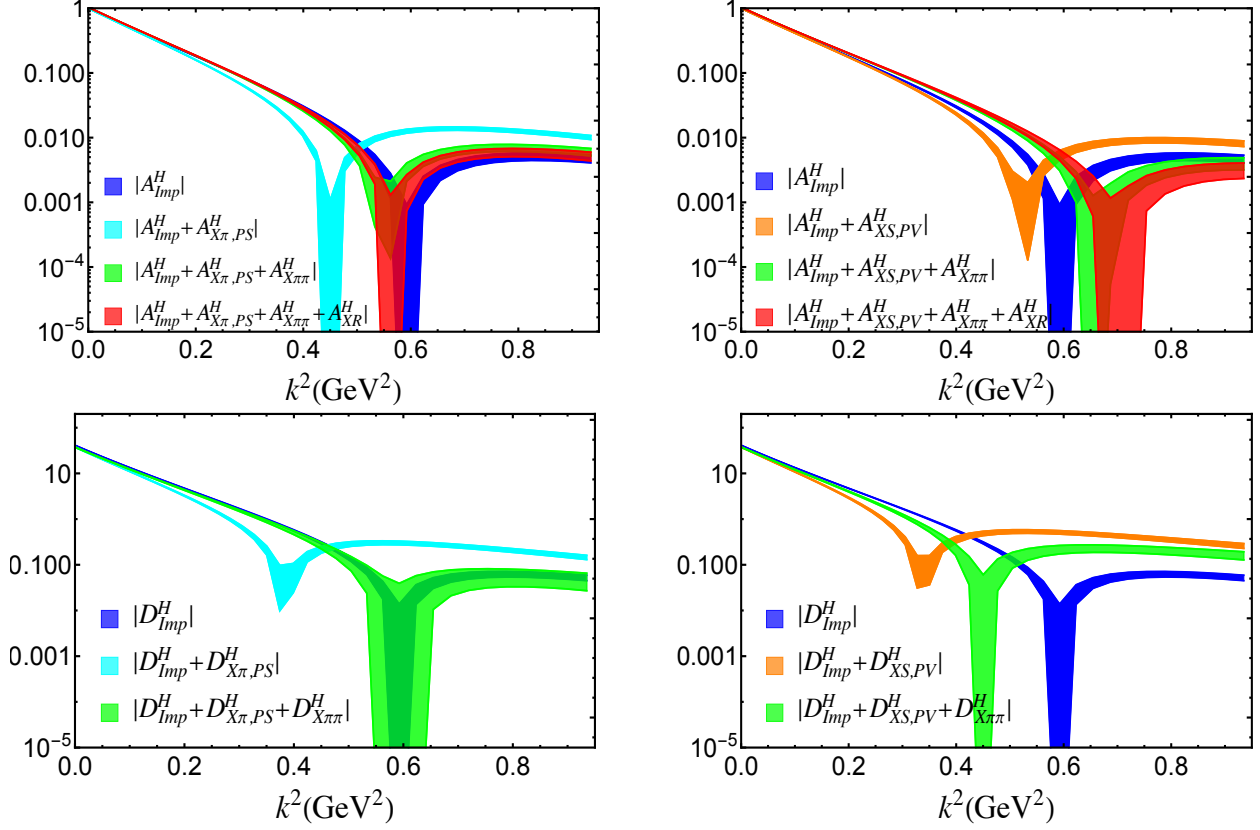


FIG. 4: Helium-4 GFFs with PS coupling (left panel) and PV coupling (right panel), using the Argonne  $v_{14}$  potential via a Monte Carlo method. The bands represent the statistical uncertainty.

### C. Pion exchange contribution

The EMT exchange contributions stemming from the one-pion exchange in the non-relativistic reduction, are equivalent whether we use the PS or PV couplings. More specifically, the pertinent operators are [41]

$$\begin{aligned}
 T_{X\pi\pi}^{00} &= -\frac{g_{\pi N}^2}{(2m_N)^2} \tau_1 \cdot \tau_2 \frac{\vec{k}^2 \vec{\sigma}_1 \cdot \vec{q}_1 \vec{\sigma}_2 \cdot \vec{q}_2}{2w_{q_1}^2 w_{q_2}^2} T_{1\pi}(k) + \frac{g_{\pi N}^2}{(2m_N)^2} \tau_1 \cdot \tau_2 \frac{\sigma_1 \cdot q_1 \sigma_2 \cdot q_2}{2} \left( \frac{1}{w_{q_2}^2} + \frac{1}{w_{q_1}^2} \right) \\
 &+ \mathcal{O}\left(\frac{g_{\pi N}^2}{m_N^4}\right), \tag{36a}
 \end{aligned}$$

$$\begin{aligned}
 T_{X\pi\pi}^{ij} &= \frac{g_{\pi N}^2}{(2m_N)^2} \tau_1 \cdot \tau_2 \left( \frac{(\vec{k}^2 \delta^{ij} - k^i k^j) \vec{\sigma}_1 \cdot \vec{q}_1 \vec{\sigma}_2 \cdot \vec{q}_2}{2w_{q_1}^2 w_{q_2}^2} T_{1\pi}(k) + \frac{(q_1^i + q_2^i)(q_1^j + q_2^j) \vec{\sigma}_1 \cdot \vec{q}_1 \vec{\sigma}_2 \cdot \vec{q}_2}{2w_{q_1}^2 w_{q_2}^2} T_{2\pi}(k) \right) \\
 &- \delta^{ij} \frac{g_{\pi N}^2}{(2m_N)^2} \tau_1 \cdot \tau_2 \frac{\sigma_1 \cdot q_1 \sigma_2 \cdot q_2 (\vec{q}_1^2 + \vec{q}_2^2 + 2m_\pi^2)}{2w_{q_1}^2 w_{q_2}^2} + \mathcal{O}\left(\frac{g_{\pi N}^2}{m_N^4}\right), \tag{36b}
 \end{aligned}$$

with the identical matrix elements

$$\begin{aligned}
 \left\langle +\frac{k}{2} \left| T_{X\pi\pi}^{00} \right| -\frac{k}{2} \right\rangle &= (m_\alpha + \frac{k^2}{4m_\alpha}) A_{X\pi\pi}^H + \frac{k^2}{4m_\alpha} D_{X\pi\pi}^H, \\
 \left\langle +\frac{k}{2} \left| T_{X\pi\pi}^{ij} \right| -\frac{k}{2} \right\rangle &= \frac{k_i k_j - \delta^{ij} k^2}{4m_\alpha} D_{X\pi\pi}^H, \tag{37}
 \end{aligned}$$

where

$$\begin{aligned}
A_{X\pi\pi}^H &= -\frac{\vec{k}^2}{\vec{k}^2 + 4m_\alpha^2} D_{X\pi\pi}^H + 6\frac{(4\pi)^2 g_{\pi N}^2}{(2m_N)^2} T_{1\pi}(k) \int_{-\frac{1}{\sqrt{2}}}^{\frac{1}{\sqrt{2}}} dt \int_0^\infty dR \int_0^{\frac{\pi}{2}} d\theta \int_0^{\frac{\pi}{2}} d\phi \mathbb{V} \left\{ \right. \\
&\quad \frac{kL_\pi u^2 \left( \sqrt{2}k^2 R t^2 Y_0^{H,\pi\pi} \cos\theta + 3L_\pi \bar{Y}_1^{H,\pi\pi} \right)}{12t m_\alpha} j_1(ktR \cos\theta) - \frac{k^2 L_\pi^2 R u^2 \bar{Y}_1^{H,\pi\pi} \cos\theta j_2(ktR \cos\theta)}{12m_\alpha} \\
&\quad \left. - \frac{k^2 u^2 Y_0^{H,\pi\pi} \left( k^2 R (2t^2 - 1) \cos\theta + 6\sqrt{2}L_\pi \right) j_0(ktR \cos\theta)}{48m_\alpha} \right\} \langle \Phi | \tau_1 \cdot \tau_2 \sigma_1 \cdot \sigma_2 | \Phi \rangle \\
&+ 6\frac{(4\pi)^2 g_{\pi N}^2}{(2m_N)^2} \int dR \int_0^{\frac{\pi}{2}} d\theta \int_0^{\frac{\pi}{2}} d\phi V \frac{m_\pi^2 u^2}{12km_\alpha R} \left\{ -2j_1\left(\frac{kR \cos\theta}{\sqrt{2}}\right) \left( k^2 r \bar{Y}_1^H + 3\sqrt{2}m_\pi Y_2^H \sec\theta \right) \right. \\
&\quad \left. + 2km_\pi R Y_2^H j_2\left(\frac{kR \cos\theta}{\sqrt{2}}\right) + 3\sqrt{2}k \bar{Y}_1^H \sec\theta j_0\left(\frac{kR \cos\theta}{\sqrt{2}}\right) \right\} \langle \Phi | \tau_1 \cdot \tau_2 \sigma_1 \cdot \sigma_2 | \Phi \rangle, \tag{38a}
\end{aligned}$$

$$\begin{aligned}
D_{X\pi\pi}^H &= 6\frac{(4\pi)^2 g_{\pi N}^2}{(2m_N)^2} T_{1\pi}(k) \int_{-\frac{1}{\sqrt{2}}}^{\frac{1}{\sqrt{2}}} dt \int_0^\infty dR \int_0^{\frac{\pi}{2}} d\theta \int_0^{\frac{\pi}{2}} d\phi \mathbb{V} \\
&\times \left\{ -\frac{m_\alpha u^2 Y_0^{H,\pi\pi} \left[ k^2 R (2t^2 - 1) \cos\theta + 6\sqrt{2}L_\pi \right] j_0(ktR \cos\theta)}{12} \right. \\
&\quad \left. + \frac{m_\alpha L_\pi u^2 j_1(ktR \cos\theta) \left( \sqrt{2}k^2 R t^2 Y_0^{H,\pi\pi} \cos\theta + 3L_\pi \bar{Y}_1^{H,\pi\pi} \right)}{3kt} \right. \\
&\quad \left. - \frac{m_\alpha L_\pi^2 R u^2 \bar{Y}_1^{H,\pi\pi} \cos\theta j_2(ktR \cos\theta)}{3} \right\} \langle \Phi | \tau_1 \cdot \tau_2 \sigma_1 \cdot \sigma_2 | \Phi \rangle \\
&+ 6\frac{(4\pi)^2 g_{\pi N}^2}{(2m_N)^2} T_{2\pi}(k) \int_{-\frac{1}{\sqrt{2}}}^{\frac{1}{\sqrt{2}}} dt \int_0^\infty dR \int_0^{\frac{\pi}{2}} d\theta \int_0^{\frac{\pi}{2}} d\phi \mathbb{V} \left\{ \right. \\
&\quad - \frac{u^2 m_\alpha j_0(ktR \cos\theta)}{54k^2} [R Y_0^{H,\pi\pi} \cos\theta (9k^4 t^2 (1 - 2t^2) + 40L_\pi^4) \\
&\quad + 2\sqrt{2}L_\pi (10L_\pi^2 (Y_0^{H,\pi\pi} + 5Y_2^{H,\pi\pi}) - 63k^2 t^2 Y_0^{H,\pi\pi})] \\
&\quad + \frac{L_\pi t u^2 m_\alpha j_1(ktR \cos\theta)}{15k} [-\sqrt{2}R \cos\theta (5k^2 (4t^2 - 1) Y_0^{H,\pi\pi} - 28L_\pi^2 Y_2^{H,\pi\pi}) - 210L_\pi \bar{Y}_1^{H,\pi\pi}] \\
&\quad - \frac{L_\pi^2 u^2 \sec^2 \theta m_\alpha j_2(ktR \cos\theta)}{756k^4 R^2 t^2} [452k^2 L_\pi^2 R^3 t^2 Y_0^{H,\pi\pi} \cos(3\theta) + 3R \cos\theta (4L_\pi^2 Y_0^{H,\pi\pi} (113k^2 R^2 t^2 - 700) \\
&\quad + 63k^4 R^2 t^2 (1 - 12t^2) \bar{Y}_1^{H,\pi\pi}) + 452\sqrt{2}k^2 L_\pi R^2 t^2 Y_0^{H,\pi\pi} + 4\sqrt{2}k^2 L_\pi R^2 t^2 \cos(2\theta) (113Y_0^{H,\pi\pi} + 124Y_2^{H,\pi\pi}) \\
&\quad + 496\sqrt{2}k^2 L_\pi R^2 t^2 Y_2^{H,\pi\pi} + 63k^4 R^3 t^2 \bar{Y}_1^{H,\pi\pi} \cos(3\theta) - 756k^4 R^3 t^4 \bar{Y}_1^{H,\pi\pi} \cos(3\theta) \\
&\quad - 4200\sqrt{2}L_\pi Y_0^{H,\pi\pi} - 21000\sqrt{2}L_\pi Y_2^{H,\pi\pi}] \\
&\quad - \frac{4\sqrt{2}L_\pi^3 t u^2 Y_2^{H,\pi\pi} R \cos\theta m_\alpha j_3(ktR \cos\theta)}{5k} \\
&\quad \left. - \frac{10L_\pi^3 u^2 m_\alpha j_4(ktR \cos\theta) \left( 2L_\pi R Y_0^{H,\pi\pi} \cos\theta + \sqrt{2}(Y_0^{H,\pi\pi} + 5Y_2^{H,\pi\pi}) \right)}{63k^2} \right\} \langle \Phi | \tau_1 \cdot \tau_2 \sigma_1 \cdot \sigma_2 | \Phi \rangle. \tag{38b}
\end{aligned}$$

Here  $L_\pi = \left[ m_\pi^2 + \left( \frac{1}{4} - \frac{t^2}{2} \right) \vec{k}^2 \right]^{1/2}$  and the shorthand Yukawa potentials are expressed as

$$\begin{aligned}
Y_0^{H,\pi\pi} &= e^{-L_\pi \sqrt{2} R \cos\theta} / (L_\pi \sqrt{2} R \cos\theta), \\
\bar{Y}_1^{H,\pi\pi} &= (1 + 1/(L_\pi \sqrt{2} R \cos\theta)) Y_0^{H,\pi\pi},
\end{aligned}$$

$$Y_2^{H,\pi\pi} = (3/(L_\pi\sqrt{2}R\cos\theta)^2 + 3/(L_\pi\sqrt{2}R\cos\theta) + 1)Y_0^{H,\pi\pi}. \quad (38c)$$

#### D. Recoil contribution

The exchange operators stemming from the recoil terms after non-relativistic reduction are also equivalent whether we use the PS or PV coupling, they can be expressed as [41]

$$T_{XR}^{00} = -\frac{g_{\pi N}^2}{(2m_N)^2}\tau_1 \cdot \tau_2 A(k) \frac{q_2 \cdot k \sigma_1 \cdot q_2 \sigma_2 \cdot q_2}{2w_{q_2}^4} + (1 \leftrightarrow 2) + \mathcal{O}\left(\frac{g_{\pi N}^2}{m_N^4}\right), \quad (39a)$$

$$T_{XR}^{ij} = \left(\frac{g_{\pi N}^2}{m_N^4}\right). \quad (39b)$$

with the corresponding matrix elements

$$\begin{aligned} \left\langle +\frac{k}{2} \left| T_{XR}^{00} \right| -\frac{k}{2} \right\rangle &= (m_\alpha + \frac{k^2}{4m_\alpha})A_{XR}^H + \frac{k^2}{4m_\alpha}D_{XR}^H, \\ \left\langle +\frac{k}{2} \left| T_X^{ij} \right| -\frac{k}{2} \right\rangle &= \frac{k_i k_j - \delta^{ij} k^2}{4m_\alpha} D_{XR}^H = \mathcal{O}\left(\frac{g_{\pi N}^2}{m_N^4}\right), \end{aligned} \quad (40)$$

and

$$\begin{aligned} A_{XR}^H &= 6 \frac{(4\pi)^2 g_{\pi N}^2}{(2m_N)^2} A(k) \\ &\times \int_0^\infty dR \int_0^{\frac{\pi}{2}} d\theta \int_0^{\frac{\pi}{2}} d\phi \mathbb{V} \frac{km_\pi^2 u^2 j_1\left(\frac{kR\cos\theta}{\sqrt{2}}\right) (\sqrt{2}m_\pi R Y_2^H \cos\theta - 5\bar{Y}_1^H)}{6m_\alpha} \langle \Phi | \tau_1 \cdot \tau_2 \sigma_1 \cdot \sigma_2 | \Phi \rangle. \end{aligned} \quad (41)$$

#### V. NUMERICAL RESULTS

To summarise, the EMT exchange contributions to Helium-4 for the PS and PV pion nucleon couplings are given by

$$\begin{aligned} T_{DX,PS}^{00} &= T_{X\pi}^{00} + T_{X\pi\pi}^{00} + T_{XR}^{00}, \\ T_{DX,PS}^{ij} &= T_{X\pi}^{ij} + T_{X\pi\pi}^{ij}, \\ T_{DX,PV}^{00} &= T_{X\pi\pi}^{00} + T_{XR}^{00}, \\ T_{DX,PV}^{ij} &= T_{XS}^{ij} + T_{X\pi\pi}^{ij}. \end{aligned} \quad (42)$$

The main difference between the PS and PV couplings, is the additional contribution from the pair diagram to the  $T^{00}$  component in the PS coupling case. A similar addition is noted in the charge form factor as in (B1). We also note that the pair diagram contribution following from the PS coupling to  $T^{ij}$ , is very similar to that of the seagull diagram (absent for the PS coupling) with PV coupling. The only difference is the extra nucleon form factor  $A(k)$  included in (27b) in comparison to (33b).

The corresponding GFFs from the exchange cur-

rents are

$$\begin{aligned} A_{X,PS}^H &= A_{X\pi,PS}^H(29a) + A_{X\pi\pi}^H(38a) \\ &\quad + A_{XR}^H(41) \\ D_{X,PS}^H &= D_{X\pi,PS}^H(29b) + D_{X\pi\pi}^H(38b) \\ A_{X,PV}^H &= A_{XS,PV}^H(35b) + A_{X\pi\pi}^H(38a) \\ &\quad + A_{XR}^H(41) \\ D_{X,PV}^H &= D_{XS,PV}^H(35c) + D_{X\pi\pi}^H(38b) \end{aligned} \quad (43)$$

To assess the pion GFFs in the pion exchange current contribution, we borrow their parameterization from the recent Lattice calculation in [1],

$$\begin{aligned} T_{1\pi}^g(k) &= \frac{0.596}{1 + \frac{\vec{k}^2}{0.677 \text{ GeV}^2}} \\ T_{1\pi}^q(k) &= \frac{0.304}{1 + \frac{\vec{k}^2}{1.44 \text{ GeV}^2}} \\ T_{2\pi}^g(k) &= \frac{0.546}{1 + \frac{\vec{k}^2}{1.129 \text{ GeV}^2}} \\ T_{2\pi}^q(k) &= \frac{0.481}{1 + \frac{\vec{k}^2}{1.262 \text{ GeV}^2}} \end{aligned} \quad (44)$$

In Fig. 3 we show the Helium-4  $A^H, D^H$  GFFs using the pion-nucleon PS coupling (left) and the pion-nucleon PV coupling (right) with the K-Harmonic method. The results from the impulse approximation (blue-dots) are labeled by "Imp" are from [34]. The various contributions labeled by " $X\pi$ ", " $XS$ ", " $X\pi\pi$ ", " $XR$ " stem from the exchange contributions illustrated in Fig. 2a for the pair contribution, in Fig. 2b for the seagull contribution, in Fig. 2c for the pi-pi contribution and in Fig. 2d for the recoil contribution, respectively. The total corrections from the exchange currents using the PS coupling (red-triangle), do not yield qualitative changes to the GFFs  $A^H$  from the impulse approximation (blue-dot). However, the contribution of the exchange currents with PV coupling yield low results compared to the impulse approximation. The difference is due to the pair contribution in Fig. 2a, whose contribution is higher order in the PV coupling. The contributions of the exchange currents to  $D^H$  are comparable in the PS and PV case, since the only difference is the extra nucleon form factor  $A(k)$  included in  $D_{X\pi,PS}^H$ , but absent in  $D_{XS,PV}^H$ . Both shift the diffractive minima to the left of the impulse approximation.

In Fig. 4 we show the Helium-4  $A^H, D^H$  GFFs using the pion-nucleon PS coupling (left) and the pion-nucleon PV coupling (right) with the Argonne  $v14$  potential. The statistical uncertainties following from the Monte-Carlo sampling, are reflected in

the colored-spreads when the various exchange contributions are added to the impulse approximation labeled by "Imp" (blue-spread) results. Again, different contributions labeled by " $X\pi$ ", " $XS$ ", " $X\pi\pi$ ", " $XR$ " stem from the exchange contributions for the pair contribution, the seagull contribution, the pi-pi contribution and the recoil contribution, respectively. Unlike the K-harmonic method, the use of the Argonne  $v14$  potential with D-wave admixture, shows sensitivity to the use of the PS (left) versus PV (right) pion-nucleon coupling. The use of the PS coupling (left) shows that the additional contributions stemming from the exchange contributions when added up (read-spread), contribute net  $A, D$  GFFs that are comparable with the impulse approximation (blue-spread) within statistics. This is not the case when using the PV coupling for the Helium-4 GFFs (right), with the net result of form factor  $A^H$  (red band) is lower than result with impulse approximation (blue-spread), the diffractive minima of form factor  $D^H$  (green-spread) is shifted to the left in comparison to that for impulse approximation (blue-spread). Again, the difference of form factor  $A^H$  stems primarily from the  $T^{00}$  component of pair diagram in the PS coupling. The difference in  $D^H$  is caused by the extra nucleon GFF  $A(k)$  in (27b) with the PS coupling, when compared to (33b) with PV coupling. In both cases, the GFF diffractive minima from the impulse approximation, shift rightward in comparison to the K-harmonic method.

## VI. CONCLUSIONS

We have analyzed the exchange contributions to the GFFs  $A, D$  for Helium-4. For that, we used a wavefunction that is maximally symmetric in the hyper-radius following from the K-harmonic method, with no D-wave admixture for simplicity. The results for the form factor  $A^H$  are overall consistent with the one we recently reported using the impulse approximation in [34], whether we use the pion-nucleon PS or PV couplings. The diffractive minima of the form factor  $D^H$  shift leftward when the exchange currents are added.

For comparison, we have also used a more realistic wavefunction following from the Argonne  $v14$  potential, with D-wave admixture. This approach is numerically intensive, and relies on Monte-Carlo sampling to generate the GFFs, with inherent statis-

tical uncertainties that can be improved with longer runs. In this case, the exchange contributions were found to be overall consistent with the impulse approximation within statistics, when the pion-nucleon PS coupling is used. When the PV coupling is used, the exchange contributions are significant.

Our analysis of the charge form factor for Helium-4 carried for comparison in Appendix B. The exchange contributions from the PS coupling to the Helium-4 charge form factor, are larger in comparison to the impulse approximation when using the Argonne  $v14$  potential, significantly improving the agreement with experiment, while the PV coupling contributions are smaller and in agreement with the impulse approximation. For both cases, the diffractive GFF minima following from the impulse approximation, shift rightward in comparison to the K-harmonic result.

r(fm)	$f_{0,1}(r)$	$f_{1,0}(r)$	$f_{t,0}(r)$
0.05	0.1644	0.2291	0
0.25	0.2626	0.3448	0.0339
0.50	0.5690	0.6491	0.0859
0.75	0.9069	0.9480	0.1264
1.00	1.0586	1.0735	0.1361
1.25	1.0512	1.0525	0.1255
1.50	0.9812	0.9694	0.1084
1.75	0.8965	0.8719	0.0916
2.00	0.8135	0.7783	0.0770
2.25	0.7369	0.6942	0.0650
2.50	0.6677	0.6203	0.0550
2.75	0.6056	0.5560	0.0469
3.00	0.5500	0.4999	0.0403
3.25	0.5002	0.4508	0.0349
3.50	0.4555	0.4077	0.0305
3.75	0.4153	0.3694	0.0268
4.00	0.3791	0.3354	0.0238
4.25	0.3464	0.3049	0.0212
4.50	0.3168	0.2775	0.0189
4.75	0.2900	0.2528	0.0169
5.00	0.2657	0.2305	0.0151
5.25	0.2436	0.2103	0.0136
5.50	0.2235	0.1920	0.0122
5.75	0.2052	0.1754	0.0109
6.00	0.1885	0.1603	0.0099
6.25	0.1733	0.1466	0.0089
6.50	0.1593	0.1341	0.0080
6.75	0.1466	0.1227	0.0072
7.00	0.1349	0.1123	0.0065
7.25	0.1242	0.1029	0.0059
7.50	0.1144	0.0943	0.0054
7.75	0.1054	0.0864	0.0049
8.00	0.0972	0.0792	0.0044
8.25	0.0896	0.0726	0.0040
8.50	0.0826	0.0666	0.0036
8.75	0.0762	0.0611	0.0033
9.00	0.0704	0.0561	0.0030
9.25	0.0650	0.0515	0.0027
9.50	0.0600	0.0472	0.0025
9.75	0.0554	0.0434	0.0023
10.00	0.0512	0.0388	0.0020

TABLE I: The wave functions  $f_{0,1}$ ,  $f_{1,0}$ ,  $f_{t,0}$  solutions to Eq. (20).

Overall, most of the exchange contributions are small in the range  $k \leq \frac{1}{2}m_N$ , leaving unchanged the mass radii. While they are separately sizable at higher momenta, fortunately their sum total is

small, with the exception of the GFFs with PV coupling used with the Argonne  $v14$  potential. Since the Helium charge form factor is better described by the PS coupling using the Argonne  $v14$  potential, we ex-

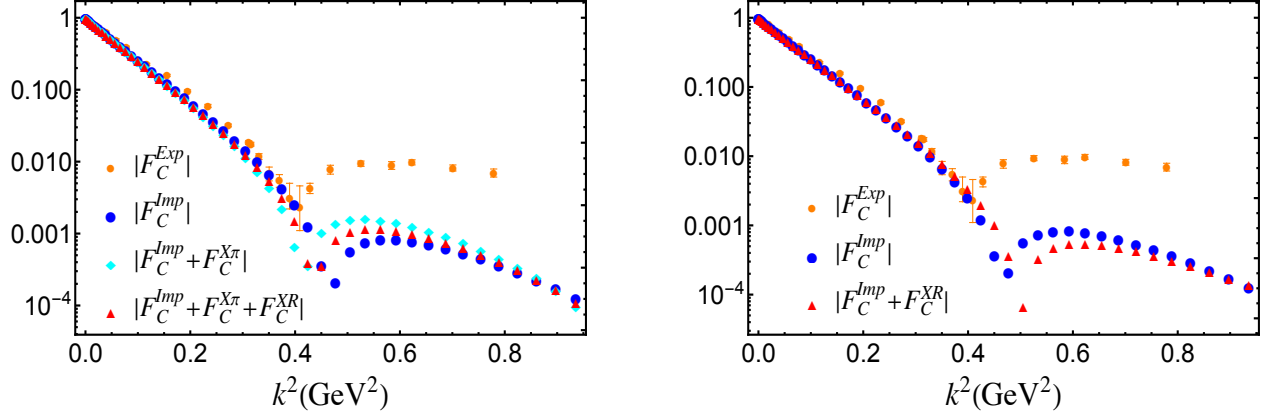


FIG. 5: Charge form factor of Helium-4 with the PS coupling(left) and PV coupling (right) using the K-Harmonics method. The subscript “imp” refers to the impulse approximation, while the subscripts “ $X\pi$ ” and “XR” refer to the exchange contributions from the pair diagram shown in Fig. 2a and recoil contribution shown in Fig. 2d, respectively. “Exp” are the experimental results for the charge form factor in [47].

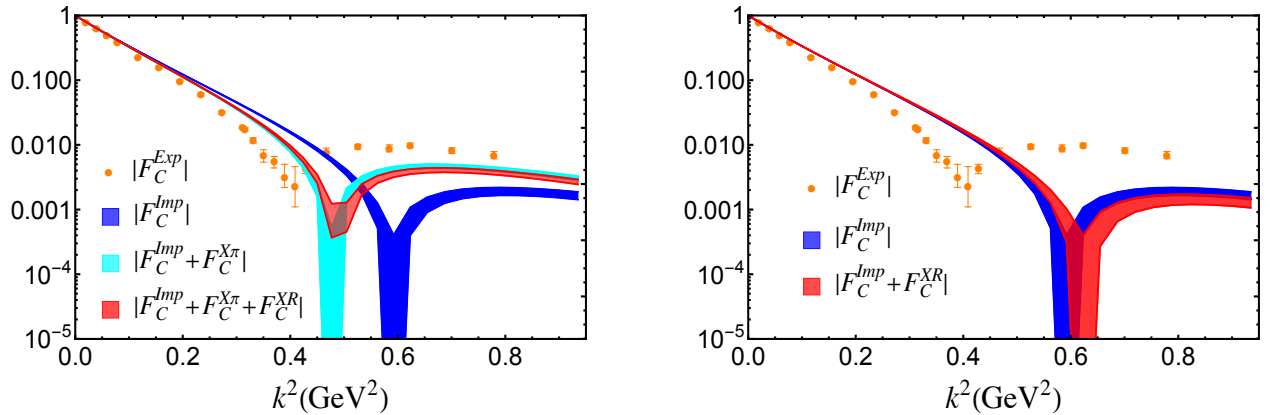


FIG. 6: The charge form factor of Helium-4 with PS coupling (left) and PV coupling (right) using the Monte Carlo method. The bands represent the statistic uncertainty. The orange data points are the experimental results in [47].

pect the PS results for the GFFs with this potential to be more reliable.

The nucleon GFFs have been recently probed at JLab [7, 8], through near threshold photoproduction of charmonium. It would be useful to extend these experiments to Helium-4, for a better understanding of the role of the exchange currents in understanding the mass distribution in light nuclei, with a particular interest in extracting the pion GFF.

### Acknowledgements

We thank Zein-Eddine Meziani and Robert Wiringa for discussions. FH is supported by the National

Science Foundation under CAREER Award PHY-1847893. IZ is supported by the Office of Science, U.S. Department of Energy under Contract No. DE-FG-88ER40388. This research is also supported in part within the framework of the Quark-Gluon Tomography (QGT) Topical Collaboration, under contract no. DE-SC0023646.

### Appendix A: Trial wave functions

In table I, we list the numerical values of three wave-functions  $f_{0,1}$ ,  $f_{1,0}$ ,  $f_{t,0}$  solution to the coupled

Schrodinger equations (20) in the regime  $r < 10$  fm. In the regime  $r > 10$  fm, we use the asymptotic expressions in [44],

$$\begin{aligned}
f_{0,1}(r > 10 fm) &= 1.88 \left( \frac{e^{-0.850961r}}{r} \right)^{\frac{1}{3}}, \\
f_{1,0}(r > 10 fm) &= 1.75 \left( \frac{e^{-0.912554r}}{r} \right)^{\frac{1}{3}}, \\
f_{t,0}(r > 10 fm) &= 0.0665 \left( 1 - e^{-\frac{r^2}{4}} \right) \\
&\quad \times \left( \frac{3.6025}{r^2} + \frac{3.28748}{r} + 1 \right) \\
&\quad \times \left( \frac{e^{-0.912554r}}{r} \right)^{\frac{1}{3}}. \tag{A1}
\end{aligned}$$

## Appendix B: Electric form factor of Helium-4

In this appendix, we summarise the results for the charge form factor for Helium-4 using the K-Harmonic method, and the trial state using the Argonne  $v14$  potential. More specifically, the leading non-relativistic form for the isoscalar electric operators for the pair diagram with PS and PV couplings are

$$\begin{aligned}
J_{X\pi,PS}^0(k) &= G_M^S \frac{g_{\pi N}^2}{(2m_N)^2} \tau_1 \cdot \tau_2 \frac{\vec{\sigma}_1 \cdot \vec{k} \vec{\sigma}_2 \cdot \vec{q}_2}{m_N w_{q_2}^2} \\
&\quad + (1 \leftrightarrow 2) + \mathcal{O}\left(\frac{g_{\pi N}^2}{m_N^4}\right), \\
J_{X\pi,PV}^0(k) &= \mathcal{O}\left(\frac{g_{\pi N}^2}{m_N^4}\right). \tag{B1}
\end{aligned}$$

The operator for the recoil correction for both PS and PV is

$$\begin{aligned}
J_{XR}^0 &= -\frac{g_{\pi N}^2}{(2m_N)^2} \tau_1 \cdot \tau_2 G_E^S \frac{q_2 \cdot k \sigma_1 \cdot q_2 \sigma_2 \cdot q_2}{2m_N w_{q_2}^4} \\
&\quad + (1 \leftrightarrow 2) + \mathcal{O}\left(\frac{g_{\pi N}^2}{m_N^4}\right), \tag{B2}
\end{aligned}$$

where  $G_M^S$  and  $G_E^S$  represent the iso-singlet combination of nucleon electric and magnetic form factors. The seagull diagram and pion exchange diagrams only contribute to the isospin vector form factor, not discussed here. The results of electric form factors can be easily obtained since the operator  $J_{X\pi,PS}^0(k)$  and  $J_{XR}^0$  are quite similar as  $T_{X\pi,PS}^{00}(k)$  and  $T_{XR}^{00}$  defined in Eq. (27a) and Eq. (39a).

In Fig. 5 we show the results for Helium-4 charge form factor with the PS pion-nucleon coupling (left) and PV pion-nucleon coupling (right) using the K-Harmonics method with no D-wave admixture. The labels are “*Imp*” (impulse approximation), “*Xπ*” (pair correction), “*XR*” (recoil correction) and “*Exp*” (experiment) from [47]. For comparison, we show in Fig. 6 the results of the Monte-Carlo simulation using the wavefunction generated from the Argonne  $v14$  potential with D-wave admixture, with the same labelings and color coding. The colored-spreads reflect on the statistical uncertainties. In the latter, the PS coupling yields a charge form factor that is in reasonable agreement with the data.

- 
- [1] Daniel C. Hackett, Patrick R. Oare, Dimitra A. Pefkou, and Phiala E. Shanahan, “Gravitational form factors of the pion from lattice QCD,” *Phys. Rev. D* **108**, 114504 (2023), [arXiv:2307.11707 \[hep-lat\]](#).
  - [2] Daniel C. Hackett, Dimitra A. Pefkou, and Phiala E. Shanahan, “Gravitational form factors of the proton from lattice QCD,” (2023), [arXiv:2310.08484 \[hep-lat\]](#).
  - [3] Bigeng Wang, Fangcheng He, Gen Wang, Terrence Draper, Jian Liang, Keh-Fei Liu, and Yi-Bo Yang ( $\chi$ QCD), “Trace anomaly form factors from lattice QCD,” *Phys. Rev. D* **109**, 094504 (2024), [arXiv:2401.05496 \[hep-lat\]](#).
  - [4] Maxim V. Polyakov and Peter Schweitzer, “Forces inside hadrons: pressure, surface tension, mechanical radius, and all that,” *Int. J. Mod. Phys. A* **33**, 1830025 (2018), [arXiv:1805.06596 \[hep-ph\]](#).
  - [5] V. D. Burkert, L. Elouadrhiri, F. X. Girod, C. Lorcé, P. Schweitzer, and P. E. Shanahan, “Colloquium: Gravitational form factors of the proton,” *Rev. Mod. Phys.* **95**, 041002 (2023), [arXiv:2303.08347 \[hep-ph\]](#).
  - [6] V. Punjabi, C. F. Perdrisat, M. K. Jones, E. J. Brash, and C. E. Carlson, “The Structure of the Nucleon: Elastic Electromagnetic Form Factors,” *Eur. Phys. J. A* **51**, 79 (2015), [arXiv:1503.01452 \[nucl-ex\]](#).
  - [7] A. Ali *et al.* (GlueX), “First Measurement of Near-Threshold  $J/\psi$  Exclusive Photoproduction off the

- Proton,” *Phys. Rev. Lett.* **123**, 072001 (2019), [arXiv:1905.10811 \[nucl-ex\]](#).
- [8] B. Duran *et al.*, “Determining the gluonic gravitational form factors of the proton,” *Nature* **615**, 813–816 (2023), [arXiv:2207.05212 \[nucl-ex\]](#).
- [9] Kiminad A. Mamo and Ismail Zahed, “Diffractive photoproduction of  $J/\psi$  and  $\Upsilon$  using holographic QCD: gravitational form factors and GPD of gluons in the proton,” *Phys. Rev. D* **101**, 086003 (2020), [arXiv:1910.04707 \[hep-ph\]](#).
- [10] Yuxun Guo, Xiangdong Ji, and Yizhuang Liu, “QCD Analysis of Near-Threshold Photon-Proton Production of Heavy Quarkonium,” *Phys. Rev. D* **103**, 096010 (2021), [arXiv:2103.11506 \[hep-ph\]](#).
- [11] H. S. Jo *et al.* (CLAS), “Cross sections for the exclusive photon electroproduction on the proton and Generalized Parton Distributions,” *Phys. Rev. Lett.* **115**, 212003 (2015), [arXiv:1504.02009 \[hep-ex\]](#).
- [12] Zainul Abidin and Carl E. Carlson, “Nucleon electromagnetic and gravitational form factors from holography,” *Phys. Rev. D* **79**, 115003 (2009), [arXiv:0903.4818 \[hep-ph\]](#).
- [13] Andrei V. Belitsky and X. Ji, “Chiral structure of nucleon gravitational form-factors,” *Phys. Lett. B* **538**, 289–297 (2002), [arXiv:hep-ph/0203276](#).
- [14] Maxim V. Polyakov and Bao-Dong Sun, “Gravitational form factors of a spin one particle,” *Phys. Rev. D* **100**, 036003 (2019), [arXiv:1903.02738 \[hep-ph\]](#).
- [15] Ho-Yeon Won, Hyun-Chul Kim, and June-Young Kim, “Flavor structure of the energy-momentum tensor form factors of the proton,” *Phys. Lett. B* **850**, 138489 (2024), [arXiv:2302.02974 \[hep-ph\]](#).
- [16] Yoshitaka Hatta, “Accessing the gravitational form factors of the nucleon and nuclei through a massive graviton,” *Phys. Rev. D* **109**, L051502 (2024), [arXiv:2311.14470 \[hep-ph\]](#).
- [17] Cédric Lorcé, “Electromagnetic and gravitational form factors of the nucleon,” in *25th International Spin Symposium* (2024) [arXiv:2402.00429 \[hep-ph\]](#).
- [18] Kiminad A. Mamo and Ismail Zahed, “ $J/\psi$  near threshold in holographic QCD: A and D gravitational form factors,” *Phys. Rev. D* **106**, 086004 (2022), [arXiv:2204.08857 \[hep-ph\]](#).
- [19] Wojciech Broniowski and Enrique Ruiz Arriola, “Gravitational and higher-order form factors of the pion in chiral quark models,” *Physical Review D* **78** (2008), 10.1103/physrevd.78.094011.
- [20] T. Frederico, E. Pace, B. Pasquini, and G. Salmè, “Pion generalized parton distributions with covariant and light-front constituent quark models,” *Physical Review D* **80** (2009), 10.1103/physrevd.80.054021.
- [21] Cristiano Fanelli, Emanuele Pace, Giovanni Romanelli, Giovanni Salmè, and Marco Salmistraro, “Pion generalized parton distributions within a fully covariant constituent quark model,” *The European Physical Journal C* **76** (2016), 10.1140/epjc/s10052-016-4101-1.
- [22] Adam Freese and Ian C. Cloët, “Gravitational form factors of light mesons,” *Physical Review C* **100** (2019), 10.1103/physrevc.100.015201.
- [23] A. F. Krutov and V. E. Troitsky, “Pion gravitational form factors in a relativistic theory of composite particles,” *Phys. Rev. D* **103**, 014029 (2021), [arXiv:2010.11640 \[hep-ph\]](#).
- [24] Khepani Raya, Zhu-Fang Cui, Lei Chang, Jose-Manuel Morgado, Craig D. Roberts, and Jose Rodriguez-Quintero, “Revealing pion and kaon structure via generalised parton distributions \*,” *Chin. Phys. C* **46**, 013105 (2022), [arXiv:2109.11686 \[hep-ph\]](#).
- [25] Yin-Zhen Xu, Minghui Ding, Khépani Raya, Craig D. Roberts, José Rodríguez-Quintero, and Sebastian M. Schmidt, “Pion and kaon electromagnetic and gravitational form factors,” *Eur. Phys. J. C* **84**, 191 (2024), [arXiv:2311.14832 \[hep-ph\]](#).
- [26] Yang Li and James P. Vary, “Stress inside the pion in holographic light-front qcd,” *Physical Review D* **109** (2024), 10.1103/physrevd.109.1051501.
- [27] Wojciech Broniowski and Enrique Ruiz Arriola, “Gravitational form factors of the pion and meson dominance,” (2024), [arXiv:2405.07815 \[hep-ph\]](#).
- [28] Wei-Yang Liu, Edward Shuryak, and Ismail Zahed, “Gluon contributions to nucleon matrix elements in the QCD instanton vacuum,” To Appear (2024).
- [29] Wei-Yang Liu, Edward Shuryak, Christian Weiss, and Ismail Zahed, “Pion gravitational form factors in the QCD instanton vacuum I,” (2024), [arXiv:2405.14026 \[hep-ph\]](#).
- [30] Ingo Sick, “Precise root-mean-square radius of He-4,” *Phys. Rev. C* **77**, 041302 (2008).
- [31] Dan Olof Riska, “EXCHANGE CURRENTS,” *Phys. Rept.* **181**, 207 (1989).
- [32] T. Mibe *et al.* (CLAS), “First measurement of coherent phi-meson photoproduction on deuteron at low energies,” *Phys. Rev. C* **76**, 052202 (2007), [arXiv:nucl-ex/0703013](#).
- [33] W. C. Chang *et al.*, “Forward coherent phi-meson photoproduction from deuterons near threshold,” *Phys. Lett. B* **658**, 209–215 (2008), [arXiv:nucl-](#)



- ex/0703034.
- [34] Fangcheng He and Ismail Zahed, “Gravitational form factors of light nuclei: Impulse approximation,” *Phys. Rev. C* **109**, 045209 (2024), arXiv:2310.12315 [nucl-th].
- [35] Alberto Garcia Martin-Caro, Miguel Huidobro, and Yoshitaka Hatta, “Gravitational form factors of nuclei in the Skyrme model,” *Phys. Rev. D* **108**, 034014 (2023), arXiv:2304.05994 [nucl-th].
- [36] J. Hockert, D. O. Riska, M. Gari, and A. Huffman, “Meson exchange currents in deuteron electrodisintegration,” *Nucl. Phys. A* **217**, 14–28 (1973).
- [37] M. Chemtob, E. J. Moniz, and Mannque Rho, “Deuteron Electromagnetic Structure at Large Momentum Transfer,” *Phys. Rev. C* **10**, 344–352 (1974).
- [38] W. M. Kloet and J. A. Tjon, “MESON EXCHANGE EFFECTS ON THE CHARGE FORM-FACTORS OF THE TRINUCLEON SYSTEM,” *Phys. Lett. B* **49**, 419–422 (1974).
- [39] A. D. Jackson, A. Lande, and D. O. Riska, “Pion exchange currents in elastic electron deuteron scattering,” *Phys. Lett. B* **55**, 23–27 (1975).
- [40] Adam Freese and Wim Cosyn, “Spatial densities of momentum and forces in spin-one hadrons,” *Phys. Rev. D* **106**, 114013 (2022), arXiv:2207.10787 [hep-ph].
- [41] Fangcheng He and Ismail Zahed, “Deuteron gravitational form factors: exchange currents,” (2024), arXiv:2401.09318 [nucl-th].
- [42] Robert B. Wiringa, R. A. Smith, and T. L. Ainsworth, “Nucleon Nucleon Potentials with and Without Delta (1232) Degrees of Freedom,” *Phys. Rev. C* **29**, 1207–1221 (1984).
- [43] J. Castilho Alcaras and B. Pimentel Escobar, “Application of the Basic Approximation of the K-Harmonics Method to the Alpha Particle,” *Revista Brasileira de Física* **4**, 83 (1974).
- [44] Robert B. Wiringa, “Variational calculations of few-body nuclei,” *Phys. Rev. C* **43**, 1585–1598 (1991).
- [45] J. Lomnitz-Adler and V. R. Pandharipande, “A simple and realistic triton wave function,” *Nucl. Phys. A* **342**, 404–420 (1980).
- [46] J. Lomnitz-Adler, V. R. Pandharipande, and R. A. Smith, “Monte Carlo calculations of triton and  $^4\text{He}$  nuclei with the Reid potential,” *Nucl. Phys. A* **361**, 399–411 (1981).
- [47] M. Garcon *et al.*, “Tensor polarization in elastic electron - deuteron scattering in the momentum transfer range  $3.8\text{-fm}^{-1} \leq q \leq 4.6\text{-fm}^{-1}$ ,” *Phys. Rev. C* **49**, 2516–2537 (1994).